J. Fluid Mech. (2013), *vol.* 727, R3, doi:10.1017/jfm.2013.267

JFM RAPIDS
journals.cambridge.org/rapids

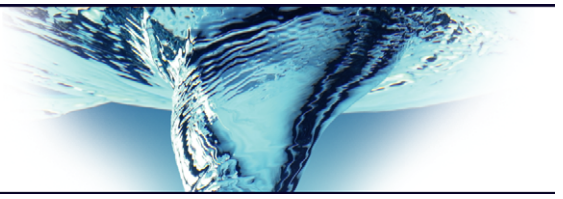

On the limitation of imposed velocity field strategy for Coulomb-driven electroconvection flow simulations

Philippe Traoré† and Jian Wu

Institut PPRIME, Boulevard Pierre et Marie Curie, BP 30179, 86962 Futuroscope-Chasseneuil, France

(Received 7 March 2013; revised 3 May 2013; accepted 23 May 2013;
first published online 26 June 2013)

This study refers to the article of Chicón, Castellanos & Martion (*J. Fluid Mech.*, vol. 344, 1997, pp. 43–66), who presented a numerical study of electroconvection in a layer of dielectric liquid induced by unipolar injection. An important characteristic of the numerical strategy proposed by Chicón *et al.* lies in the fact that the Navier–Stokes equations are never solved to obtain the velocity field, which is subsequently needed in the charge density transport equation. Instead, the velocity field is explicitly provided by an expression obtained with some assumptions about the flow structure and related to the electric field (the imposed velocity field approach; IVF). The validity of the above simplification is examined through a direct comparison of the solutions obtained by solving the Navier–Stokes equations (the Navier–Stokes computation approach; NSC). It is clearly demonstrated that, even in the strong injection regime ($C = 10$), the results look very similar for a given range of the mobility parameter M; however, in the weak injection regime ($C = 0.1$), significant discrepancies are observed. The rich flow structures obtained with the NSC approach invalidate the use of the IVF approach in the weak injection regime.

Key words: computational methods, convection, MHD and electrohydrodynamics

1. Introduction

In the configuration considered in the study of Chicón, Castellanos & Martion (1997), when the applied voltage is high enough, the Coulomb force gives rise to the development of an instability that puts the liquid into motion in the form of electroconvective rolls. This strong and nonlinear coupling, as well as the complexity of the mathematical problem, has prevented the development of any analytical solution.

† Email address for correspondence: philippe.traore@univ-poitiers.fr

This inherent complexity has encouraged the use of numerical methods to gain additional insight into physical phenomena. The first attempt to solve the whole coupled system of partial differential equations with adequate numerical methods was conducted by Castellanos & Atten (1987) and Castellanos, Atten & Perez (1987). The authors solved the Navier–Stokes equations using the finite difference method on a staggered grid combined with the SIMPLER algorithm (Patankar 1980). The charge density transport equation was solved using the finite difference method and the upwind differencing scheme for the convective term. However, the lack of precision in their results made them change their method of solving the charge density transport equation.

By neglecting the diffusion mechanism of charge transport, the charge density equation becomes hyperbolic, and specific numerical schemes should be adopted due to the noticeably steep gradients in the charge density distribution. Chicón *et al.* (1997) developed an original particle-in-cell (PIC) method, which involves injecting numerically charged particles in the bulk. Both weak and strong injection regimes were considered. Vazquez, Georghiou & Castellanos (2006) compared the PIC method to the integration of the charge density transport equation based on the flux-corrected transport (FCT) scheme (Boris & Book 1973). However, in these papers the authors tried to uncouple the complexity of the problem and only focus on the charge density computation. Thus, the fluid velocity field is not computed from the Navier–Stokes equations. Instead, the authors assumed that the flow adopts a convective roll structure. The velocity field is then deduced from an analytical expression given by the stream function associated with this roll structure. It is interesting to note that such a simplification is quite popular in the numerical simulation of finite-amplitude electroconvection due to unipolar injection (Castellanos & Atten 1987; Castellanos *et al.* 1987; Chicón *et al.* 1997; Chicón, Perez & Castellanos 2002, 2003; Vazquez *et al.* 2006; Vazquez & Castellanos 2011).

Despite the fact that it was later successfully solved by some authors (Vazquez, Georghiou & Castellanos 2008; Kourmatzis & Shrimpton 2012; Traoré & Perez 2012), the full and complete set of equations associated with electroconvective phenomena, as well as the limitations and drawbacks of the imposed velocity field (IVF) strategy, have never been reported.

The present paper reports on the limitations of the IVF with respect to the approach of solving the full Navier–Stokes equations (the Navier–Stokes computation approach; NSC). It is demonstrated that the use of the IVF approach may lead to completely different results from those obtained with the NSC approach, especially in the weak injection regime.

This paper is organized as follows. In the next section, the governing equations and the numerical background used in the two approaches (NSC and IVF) are introduced and described. Detailed and exhaustive numerical results are presented in § 3. Finally, a conclusion is provided in § 4.

2. Governing equations and numerical background

2.1. *Governing equations*

The system under consideration is a dielectric liquid layer of width H enclosed between two electrodes of length L (figure 1). The emitter electrode is at the bottom side of the cavity. The layer is subjected to a potential difference $\Delta V = V_0 - V_1$, which will inject charges from the emitter electrode into the bulk. The injection is assumed to be *homogeneous* and *autonomous*.

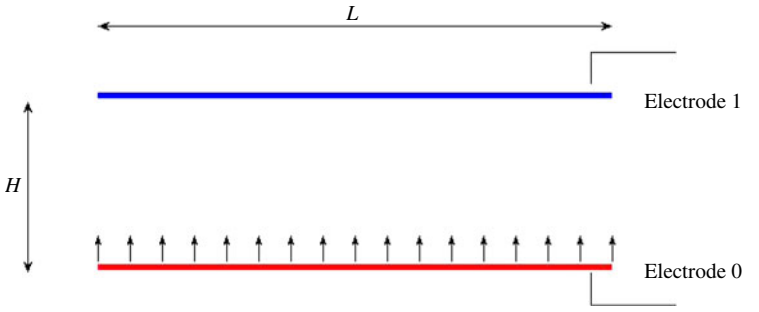

FIGURE 1. Sketch of the physical domain.

The governing equations of such a problem are ruled by the electrohydrodynamic (EHD) equations, which is a set of coupled partial differential equations including the Navier–Stokes equations, the charge density transport equation and Gauss's law for the electrostatic potential. These equations can be written in dimensionless form using the scales H, (V_0-V_1), $\varepsilon(V_0-V_1)/H^2$ and $K(V_0-V_1)/H$ for, respectively, length, potential, charge density and velocity. Here ε and K stand for the permittivity and ionic mobility, respectively (Chicón *et al.* 1997). Thus we have

$$\nabla \cdot \boldsymbol{v} = 0, \tag{2.1}$$

$$\frac{\partial \boldsymbol{v}}{\partial t} + (\boldsymbol{v} \cdot \nabla)\boldsymbol{v} = -\nabla \tilde{p} + \frac{M^2}{T}\Delta \boldsymbol{v} + M^2 q\boldsymbol{E}, \tag{2.2}$$

$$\frac{\partial q}{\partial t} + \nabla \cdot (q(\boldsymbol{v} + \boldsymbol{E})) = 0, \tag{2.3}$$

$$\Delta V = -q, \tag{2.4}$$

where $\boldsymbol{v} = [u, v]$ is the fluid velocity, q is the charge density, $\boldsymbol{E}$ is the electric field, V is the electric potential and $\tilde{p}$ is the modified pressure, which includes the pressure and the scalar term from which the electrostriction force is derived. As the fluid is homogeneous and isothermal, the dielectric force vanishes and only the Coulomb force $q\boldsymbol{E}$ acts on the fluid.

Three dimensionless numbers arise in the equations:

$$T = \frac{\varepsilon \Delta V}{\rho_0 \nu K}, \quad C = \frac{q_0 H^2}{\varepsilon \Delta V}, \quad M = \frac{1}{K}\left(\frac{\varepsilon}{\rho_0}\right)^{1/2}, \tag{2.5}$$

where T represents the ratio of Coulomb and viscous forces. Felici (1969) established the existence of a linear stability criterion T_c associated with the growth of infinitely small-amplitude perturbations. The existence of another stability criterion T_f $(T_f < T_c)$, corresponding to finite-amplitude velocity disturbances, was also highlighted, which indicated the existence of a subcritical bifurcation characterized by a typical hysteresis loop.

In the above, C is a dimensionless measure of the injection strength level, while M, the mobility parameter, is the ratio between the so-called hydrodynamic mobility and the true ion mobility K. M depends only on fluid properties, with typical values for dielectric liquids lying in the range $[3, \infty[$. In parameters T and M, ρ_0 and ν stand, respectively, for the density and kinematic viscosity of the fluid.

2.2. *Derivation and numerical methods*

In the IVF approach, the fluid motion is assumed to be two-dimensional, in the form of one roll. The velocity field is given by $\boldsymbol{v} = A(t, \boldsymbol{E}, q)\,\boldsymbol{v}_0$, where $A(t, \boldsymbol{E}, q)$ is the amplitude of the velocity field, which is a function of time and the electric field and

$$\boldsymbol{v}_0 = \left(\frac{\partial \psi_0}{\partial y}, -\frac{\partial \psi_0}{\partial x} \right)^{\mathrm{T}}, \tag{2.6}$$

where $\psi_0(x, y) = (L/2\pi)(1 - \cos 2\pi y)\sin(\pi x/L)$ is the stream function, which represents one convective cell structure contained within length L.

The derivation of the amplitude equation describing the time evolution of $A(t, \boldsymbol{E}, q)$ is detailed in Chicón *et al.* (1997).

Given A^n, q^n and $\boldsymbol{E}^n$, the amplitude function, the charge density and the electric field at time step n, the amplitude at time step $n + 1$ can be expressed as

$$A^{n+1} = A^n + \Delta t \left(\frac{M^2}{T} c_1 A^n + c_2 M^2 \int_{cell} q^n \boldsymbol{v}_0 \cdot \boldsymbol{E}^n \,\mathrm{d}x\,\mathrm{d}y \right), \tag{2.7}$$

where

$$\left.\begin{aligned} c_1 &= \int_{cell} \|\boldsymbol{v}_0\|^2 \,\mathrm{d}x\,\mathrm{d}y = \frac{L^3}{4} + \frac{3L}{16}, \\ c_2 &= \int_{cell} \boldsymbol{v}_0 \cdot \Delta \boldsymbol{v}_0 \,\mathrm{d}x\,\mathrm{d}y = -\pi^2 \left(L^3 + \frac{L}{2} + \frac{3}{16L} \right). \end{aligned}\right\} \tag{2.8}$$

Once the amplitude A^{n+1} is determined, the velocity field is obtained with (2.6), and equations (2.3) and (2.4) can be solved, leading, respectively, to the charge density q^{n+1} and the electric potential V^{n+1}. Then $\boldsymbol{E}^{n+1} = -\boldsymbol{\nabla} V^{n+1}$ can be computed for the next time step $n + 1$.

It should be noted that the accuracy of the IVF approach can only be guaranteed on the condition that T is close to the linear stability criterion T_c.

The NSC approach involves directly solving the Navier–Stokes equations, and couples the obtained velocity field to the electrostatic equations. We developed a numerical algorithm for such incompressible flow based on the finite-volume method (Patankar 1980). The velocity–pressure coupling algorithm is undertaken by the augmented Lagrangian method (Fortin & Glowinski 1983) associated with the Uzawa algorithm (Uzawa 1958). The key when solving the charge density equation is the choice of the appropriate numerical scheme for solving hyperbolic equations. This specific aspect related to total variation diminishing (TVD) schemes will not be emphasized in this paper, since the way the charge density transport equation is solved is similar for both the NSC and IVF methods. Indeed, only the computation of the velocity field differs in the comparisons that are undertaken in this paper.

In all cases the second-order SMART (smooth monotonic algorithm for real transport) scheme of Gaskel & Lau (1988) is chosen for computing the charge density distribution. For interested readers, additional details concerning the implementation of SMART can be found in Traoré & Perez (2012).

Our numerical approach has been successfully validated for the cases of the electroconvection problem due to strong unipolar injection (Traoré & Perez 2012) and electrothermoconvective phenomena due to both injection and thermal gradient (Traoré *et al.* 2010).

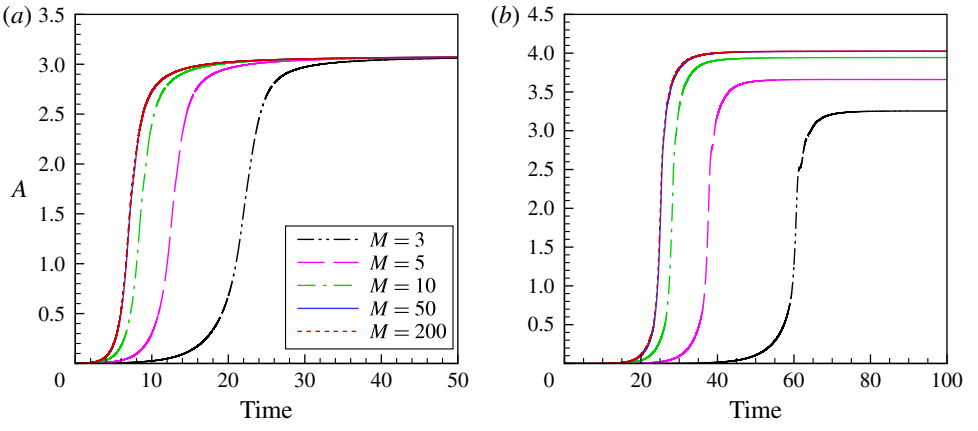

FIGURE 2. Amplitude versus time for various M values, $C = 10$ and $T = 178$: (*a*) IVF; (*b*) NSC.

To conclude this section, we finally introduce the boundary conditions that have been considered:

for $x = 0$ and $x = L$: $u = 0$; $\partial v/\partial x = 0$; $\partial q/\partial x = 0$; $\partial V/\partial x = 0$;

for $y = 0$: $u = 0$; $v = 0$; $q = C$; $V = 1$;

for $y = 1$: $u = 0$; $v = 0$; $\partial q/\partial y = 0$; $V = 0$.

We have chosen no-slip boundary conditions on the electrodes and symmetric boundary conditions in the horizontal direction to fit exactly the same boundary conditions that Chicón *et al.* (1997) have implemented in their paper. It is very common for numerical simulations undertaken in electroconvection in a horizontal layer to use such lateral boundary conditions (Castellanos *et al.* 1987; Vazquez *et al.* 2008)

Moreover, following Perez & Castellanos (1989), LeVeque (2002), Vazquez *et al.* (2008) and Kourmatzis & Shrimpton (2012), due to the practical implementation, we have used an additional condition, namely $\partial q/\partial y = 0$ on the collector electrode.

3. Results and discussion

3.1. *Strong injection regime* $C = 10$

In all the numerical computations conducted in this paper, the length of the domain is set to half of the wavelength of the most unstable mode. This wavelength has been determined by linear stability analysis for several values of the injection parameter C (Atten & Moreau 1972). Typical values of L in the strong ($C = 10$) and weak ($C = 0.1$) injection regimes are 0.614 and 0.687, respectively.

In this paper, the flow structure obtained with two different strategies for computing the velocity field is carefully analysed with regard to the M parameter, which is varied over a wide range [3, 200].

In figure 2 the time history of the velocity amplitude A for various M values is displayed. It is noted that the time development of the instability is similar for both IVF and NSC strategies. After an exponential growth period, a steady state with one cell structure is reached. We also noticed that the magnitude of A obtained at steady state is almost the same for all M in the IVF approach, as expected for this method. In the NSC approach, the scenario is bit different, and two cases must be considered. Indeed, for $M > 10$, the amplitude at steady state remains constant with M and close

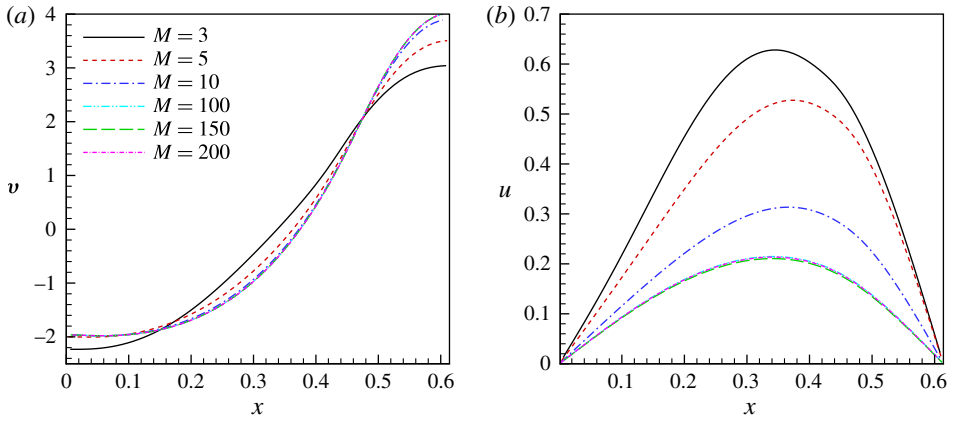

FIGURE 3. Velocity profiles in the vertical mid-section for different M values, $C = 10$ and $T = 178$: (a) vertical component profile; (b) longitudinal component profile.

to the value found using the IVF method. However, for $M \leqslant 10$, the amplitude at steady state decreases with decreasing M. This can be explained by recalling the dimensionless form of the momentum equation:

$$\frac{\partial \boldsymbol{v}}{\partial t} + (\boldsymbol{v} \cdot \nabla)\boldsymbol{v} = -\nabla \tilde{p} + \frac{M^2}{T}\Delta \boldsymbol{v} + M^2 q\boldsymbol{E} = -\nabla \tilde{p} + M^2 \left(\frac{1}{T}\Delta \boldsymbol{v} + q\boldsymbol{E}\right). \quad (3.1)$$

For high M, the term $M^2((1/T)\Delta \boldsymbol{v} + q\boldsymbol{E})$ is dominant compared to the convective or inertial term $(\boldsymbol{v} \cdot \nabla)\boldsymbol{v}$, and thus the flow becomes independent of M when steady state is reached, as predicted by the stability analysis and well reproduced by the IVF method. Only the transient phase will exhibit different behaviour. This is readily observed in figure 2(a). However, for small M $(3, 5, 10)$, the two terms $M^2((1/T)\Delta \boldsymbol{v} + q\boldsymbol{E})$ and $(\boldsymbol{v} \cdot \nabla)\boldsymbol{v}$ are of the same order and M plays a more significant role, which affects the resulting velocity distribution. As a consequence, the steady state is no longer independent of M, as can be seen in figure 2(b).

This is due to the fact that for small M the velocity distribution becomes M-dependent, while this is not the case for large M. This result is clearly depicted in figure 3, where we have plotted the vertical and longitudinal velocity profiles in the vertical mid-section $y = 0.5$. Indeed, for $M = 100$, 150 and 200, the velocity profiles are merged, while for $M = 3$, 5 and 10 different profiles are observed.

In the strong injection regime, since for all M values a final steady state is reached with similar flow structures, we choose $M = 40$ as a representative example in the following numerical experiments. In figure 4 we have depicted the stream function and charge density isocontours. In both cases, the two strategies are able to reproduce the charge-free region, which is a characteristic feature of Coulomb-driven electroconvection flows. However, the respective shapes of this charge-free region for the two cases exhibit slight differences, which are a direct consequence of the way the velocity field is computed. The main difference between the two approaches is also highlighted in the stream function, which is more symmetric in the IVF case compared to the NSC case. It can be observed that the stream function in the NSC case is tighter on the left side. This indicates an increase in the velocity magnitude in that region, whereas the velocity is symmetrically distributed across the whole domain in the IVF case.

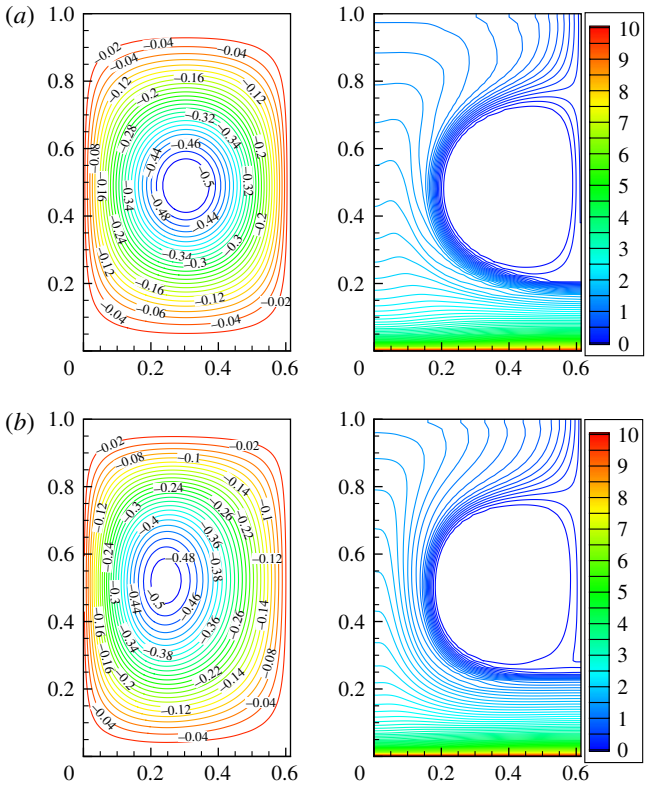

FIGURE 4. Stream function and charge density isocontours for $T = 178$ and $M = 40$: (*a*) IVF; (*b*) NSC.

Figure 5 emphasizes the subcritical bifurcation highlighted by the hysteresis loop, which is another important feature of electroconvective motion. Both IVF and NSC approaches are able to characterize the linear and nonlinear criteria T_c and T_f. For linear stability criteria, the numerical values with the IVF and NSC approaches are 162.5 and 163.2, which are remarkably close to the value (164.1) predicted by the stability analysis (Atten & Moreau 1972).

For nonlinear stability criteria, the numerical values predicted by the IVF and NSC approaches are 120.5 and 109.5, respectively. These results should be compared with the analytical value of T_f (111.7) obtained with a Galerkin method (Atten & Lacroix 1979). The accuracy in the determination of the nonlinear value T_f is directly related to the existence, shape and dynamics of the charge-free region in the charge density field (Castellanos *et al.* 1987).

Although the IVF strategy cannot accurately estimate the nonlinear stability criteria, this approach is able to capture the main characteristics of electroconvection in a strong injection regime typically when M is larger than 50.

3.2. *Weak injection regime* $C = 0.1$

In this section the numerical experimentation concerns the weak injection regime with $C = 0.1$. In figure 6 the time history of the velocity amplitude for different M values is depicted.

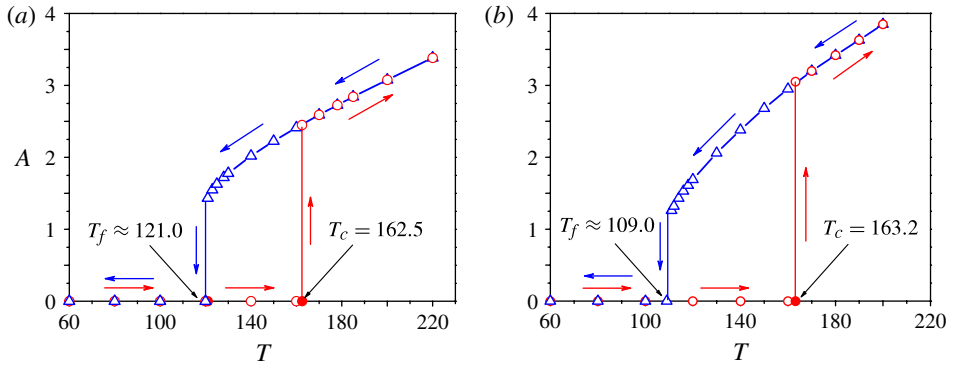

FIGURE 5. Hysteresis loops for $C = 10$ and $M = 40$ with: (*a*) IVF; and (*b*) NSC.

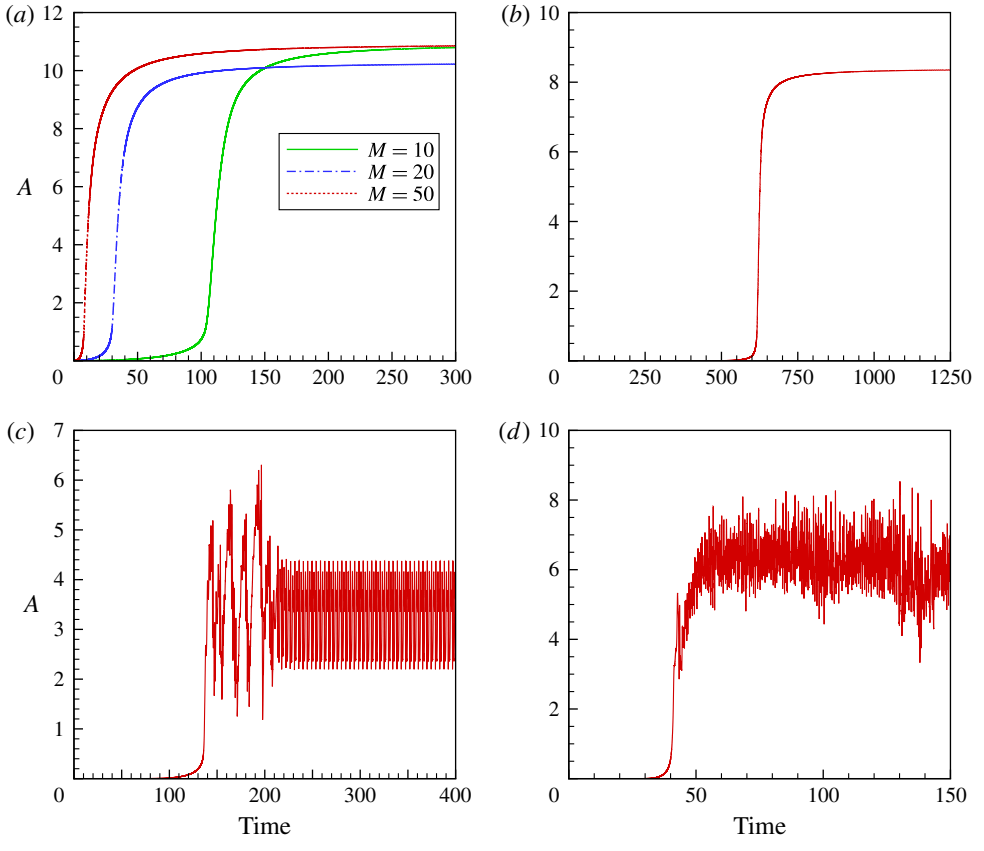

FIGURE 6. Amplitude versus time for various M values, $C = 0.1$ and $T = 30\,000$: (*a*) IVF; (*b*) NSC, $M = 10$; (*c*) NSC, $M = 20$; (*d*) NSC, $M = 50$.

Note that the IVF or NSC approaches yield completely different time developments of the instability. In the case of the IVF strategy, the time developments of the amplitude for various M are similar to those observed in the strong injection case. A steady-state one-cell structure can always be reached. However, with the NSC

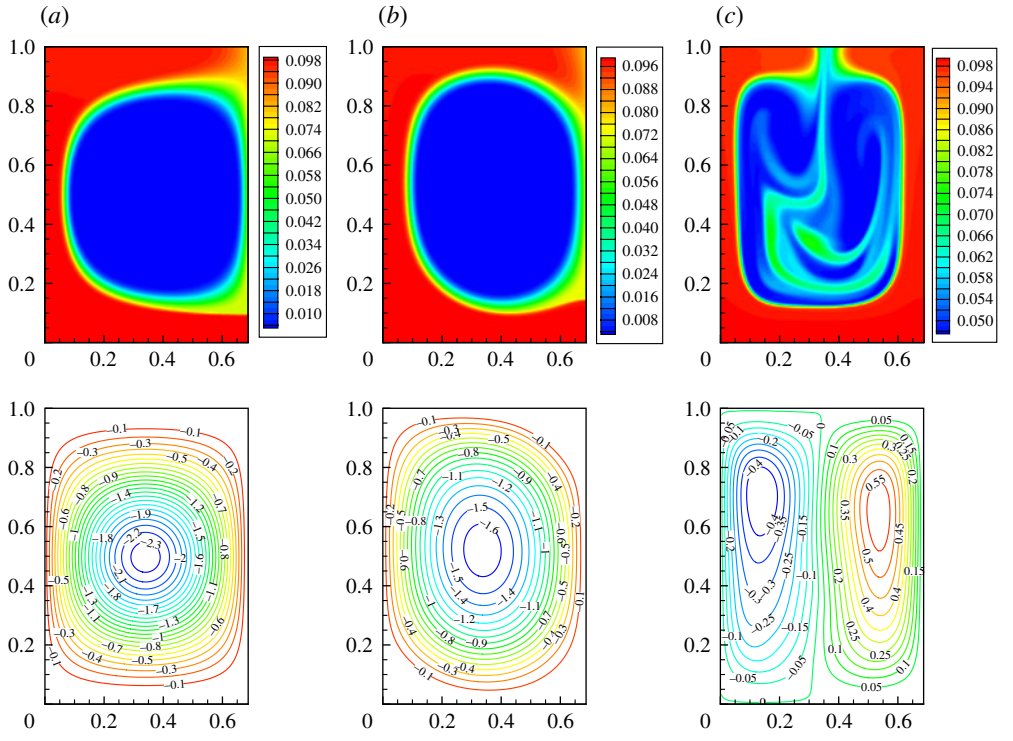

FIGURE 7. Stream function and charge density isocontours for $C = 0.1$ and $T = 30\,000$: (*a*) IVF, $M = 10$; (*b*) NSC, $M = 10$; (*c*) NSC, $M = 50$.

approach, the final steady states exhibit different characteristics, which are strongly dependent on M. For $M = 10$ we observe a steady state; for $M = 20$, a regular periodic state is reached after an irregular oscillation transition period; and for $M = 50$, the signal is strongly unsteady and appears to be chaotic. Apparently, in the weak injection regime, the IVF approach is totally invalid since it is not able to capture the unsteadiness of the flow over a wide range of the M parameter.

The charge density distribution and stream function contours are depicted in figure 7. For the case $M = 10$ (see figure 7*a*,*b*), the two solutions are of the same order and just slightly different. A more significant discrepancy occurs for $M = 50$. For this case, a two-cell structure occurs (see figure 7*c*), and this behaviour has already been reported by Vazquez *et al.* (2008). It is interesting to note that such a chaotic two-cell structure is similar to the fully chaotic regime when inertial effects are dominant in the strong injection case (Traoré & Perez 2012).

For $T = 24\,500$, which is very close to the analytical T_c value (24 147.57; Atten & Moreau 1972), a steady state was expected. In contrast, the numerical results obtained by the NSC approach show a very chaotic unsteady state (figure 8*a*). It is surprising to note that, even very close to the threshold T_c, the flow went from a motionless state to a chaotic one without crossing an intermediate steady state. A spectral analysis of the fluctuations of the velocity amplitude confirms the chaotic behaviour, by a broadband spectrum (figure 8*b*) with an exponential decay. Such an interesting phenomenon has been predicted and explained by Atten & Elouadie (1995). In their analysis, they thought that the critical T parameter with weak injection was so high that the non-

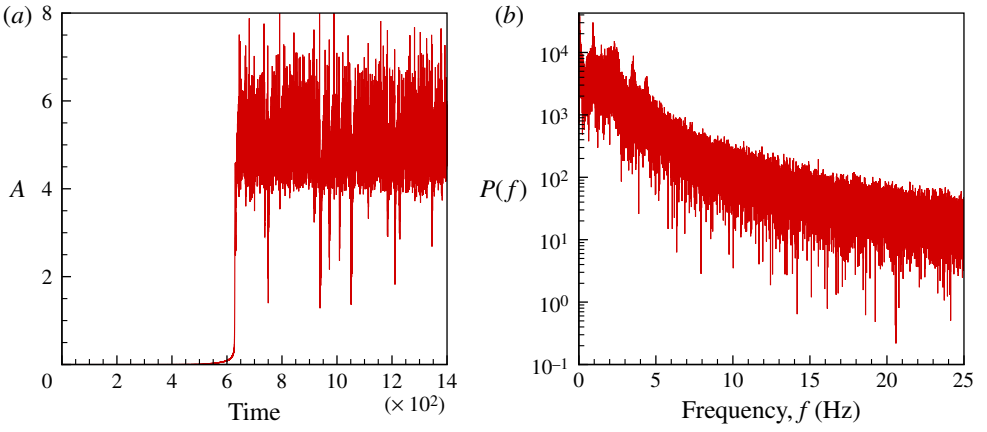

FIGURE 8. (*a*) Time evolution of the velocity amplitude for $C = 0.1$, $M = 50$ and $T = 24\,500$. (*b*) The corresponding semilog plot of power spectra curve.

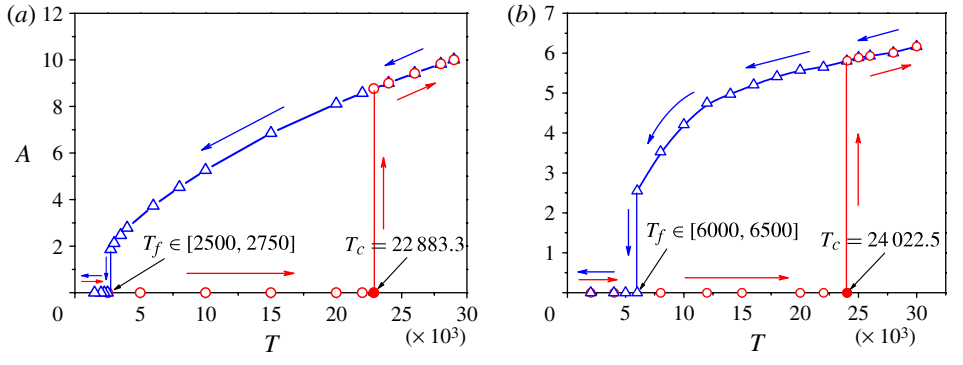

FIGURE 9. Hysteresis loops for a weak injection system ($C = 0.1$, $M = 50$) with: (*a*) IVF; (*b*) NSC.

dimensional electric Reynolds number $R = T/M^2$ was greater than the transition value (a reference value is 10) between the regions dominated by the viscous effect and the inertial effect. Our numerical findings here support their viewpoint.

Figure 9 displays the hysteresis loop obtained with the IVF and NSC approaches for $M = 50$. In the weak injection regime, the linear criterion T_c is more accurately determined with the NSC approach. However, the nonlinear value T_f is nearly twice as high as the value predicted by the expression $T_f = T_c C$ developed by Felici (1969) with his hydraulic model, which should give 2417.4.

In their paper, Chicón *et al.* (1997) have found a T_f value close to the result predicted by the hydraulic model. Our results obtained with the IVF approach are consistent with those of Chicón *et al.* (1997) (see figure 9*a*). However, this apparent agreement is misleading. Indeed, the inertial regime observed in weak injection for $M = 50$, which neither the IVF approach nor the hydraulic model can reproduce, explains the discrepancy noticed in the T_f value. This inertial regime is ascribed to the interaction of the two cells observed in the case of the NSC approach. The T_f value determined by the NSC approach is consistent with the kind of regime highlighted in weak injection. Indeed, the two-cell structure induces a strongest mixing in the charge

density distribution and the charge-free region is less stable and also thinner. As a result the flow loses its stability sooner and the T_f value will be greater compared to a flow with only a one-cell structure. The accuracy of the criteria for the numerical determination of T_c and T_f can be improved by controlling the numerical diffusion. The key parameters are the grid resolution, the time step and the numerical scheme employed for solving the charge density transport equation. The accuracy of the determination of T_f is particularly sensitive (unlike T_c) to these sources of numerical diffusion.

It is worth mentioning that, as the regime is strongly unsteady, the amplitude A in figure 9(*b*) for a given T is averaged over the whole time period of the simulation.

In fact the IVF approach cannot capture the complex flow structure characteristic of cases in which M is higher than 20. So this assumption that the velocity field would adopt a one-cell electroconvective structure is wrong for moderate values of M. We found from our computations that the flow adopts a one-cell convective structure only over a narrow range $M \in [5, 10]$.

The reason why the IVF method fails in weak injection, whereas acceptable results may be obtained in strong injection, is linked to the fact that nonlinear effects are more dominant in weak injection, especially for high M values. The complexity and richness of the flow motion in this case, which are the consequences of the development of nonlinear effects, cannot be described with a one-cell structure.

4. Conclusion

In this paper, the validity of the numerical strategy proposed by Chicón *et al.* (1997) to solve electroconvection flows between two parallel plates has been meticulously examined using several selected numerical experiments.

The numerical solutions obtained with such a simplified approach were directly compared to those obtained by solving the entire set of Navier–Stokes equations. Both strong and weak injection cases were considered. It is shown that, in the strong injection regime, the IVF approach can lead to consistent results compared to those obtained from solving the Navier–Stokes equations. However, in weak injection we have observed different behaviour that depends strongly on the M parameter, and that the IVF was completely unable to capture. For $M = 50$, the flow structure is made of two electroconvective cells that interact together in a strongly chaotic manner.

Although agreement has been corroborated only over a narrow range of M values [5, 10], we point out that the IVF approach is totally unsuited to moderate M values, and its use cannot be recommended in the numerical simulation of Coulomb-driven convection in weak injection regimes.

Acknowledgements

This work was partially funded by the French Government program Investissements d'Avenir (LABEX INTERACTIFS, reference ANR-11-LABX-0017-01), and by a grant from the French district Poitou–Charentes.

References

Atten, P. & Elouadie, L. 1995 EHD convection in a dielectric liquid subjected to unipolar injection: coaxial wire/cylinder geometry. *J. Electrostat.* **34**, 279–297.

Atten, P. & Lacroix, J. C. 1979 Non-linear hydrodynamic stability of liquids subjected to unipolar injection. *J. Méc.* **18**, 469–510.

ATTEN, P. & MOREAU, R. 1972 Stabilité électrohydrodynamique des liquides isolants soumis à une injection unipolaire. *J. Méc.* **11** (3), 471–521.

BORIS, J. P. & BOOK, D. L. 1973 Flux corrected transport I: a fluid transport algorithm that works. *J. Comput. Phys.* **11**, 38–69.

CASTELLANOS, A. & ATTEN, P. 1987 Numerical modelling of finite amplitude convection of liquids subjected to unipolar injection. *IEEE Trans. Ind. Applics.* **IA-23**, 825–830.

CASTELLANOS, A., ATTEN, P. & PEREZ, A. T. 1987 Finite amplitude electroconvection in liquid in the case of weak unipolar injection. *Physico-Chem. Hydrodyn.* **9** (3/4), 443–452.

CHICÓN, R., CASTELLANOS, A. & MARTION, E. 1997 Numerical modelling of Coulomb-driven convection in insulating liquids. *J. Fluid Mech.* **344**, 43–66.

CHICÓN, R., PEREZ, A. T. & CASTELLANOS, A. 2002 Modelling the finite amplitude electroconvection in cylindrical geometry: characterization of chaos. In *Annual Report: Conference on Electrical Insulation and Dielectric Phenomena (CEIDP), Cancun 20th–24th October 2002, IEEE conference publications*, pp. 212–215.

CHICÓN, R., PEREZ, A. T. & CASTELLANOS, A. 2003 Electrovection in small cylindrical cavities. In *Annual Report: Conference on Electrical Insulation and Dielectric Phenomena (CEIDP), Albuquerque 19th–22th October 2003, IEEE conference publications*, pp. 710–713.

FELICI, N. 1969 Phénomènes hydro et aérodynamiques dans la conduction des diélectriques fluides. *Rev. Gén. Electricité* **78**, 717–734.

FORTIN, M. & GLOWINSKI, R. 1983 *Augmented Lagrangian Methods*. North-Holland.

GASKEL, P. H. & LAU, A. K. C. 1988 Curvature-compensated convective transport: SMART, a new boundedness-preserving transport algorithm. *Intl J. Numer. Meth. Fluids* **8**, 617–641.

KOURMATZIS, A. & SHRIMPTON, J. S. 2012 Turbulent three-dimensional dielectric electro-hydrodynamic convection between two plates. *J. Fluid Mech.* **696**, 228–262.

LEVEQUE, R. J. 2002 *Finite Volume Methods for Hyperbolic Problems*. Cambridge University Press.

PATANKAR, S. V. 1980 *Numerical Heat Transfer and Fluid Flow*. McGraw-Hill.

PEREZ, A. T. & CASTELLANOS, A. 1989 Role of charge diffusion in finite-amplitude electroconvection. *Phys. Rev.* A **40** (10), 5844–5855.

TRAORÉ, P. & PEREZ, A. T. 2012 Two-dimensional numerical analysis of electroconvection in a dielectric liquid subjected to strong unipolar injection. *Phys. Fluids* **24**, 037102.

TRAORÉ, P., PEREZ, A. T., KOULOVA-NENOVA, A. D. & ROMAT, H. 2010 Numerical modelling of finite amplitude electro-thermo-convection in a dielectric liquid layer subjected to both unipolar injection and temperature gradient. *J. Fluid Mech.* **658**, 279–293.

UZAWA, H. 1958 Iterative methods for concave programming. In *Studies in Linear and Nonlinear Programming* (ed. K. J. Arrow, L. Hurwicz & H. Uzawa), pp. 154–165. Stanford University Press.

VAZQUEZ, P. A. & CASTELLANOS, A. 2011 Stability analysis of the 3D electroconvective charged flow between parallel plates using the particle-in-cell method. In *IEEE International Conference on Dielectric Liquids (ICDL), Throndheim 26th–30th June 2011*, pp. 1–4.

VAZQUEZ, P. A., GEORGHIOU, G. E. & CASTELLANOS, A. 2006 Characterization of injection instabilities in electrohydrodynamics by numerical modelling: comparison of particle in cell and flux corrected transport methods for electroconvection between two plates. *J. Phys.* D: *Appl. Phys.* **39**, 2754–2763.

VAZQUEZ, P. A., GEORGHIOU, G. E. & CASTELLANOS, A. 2008 Numerical analysis of the stability of the electro-hydrodynamic (EHD) electroconvection between two plates. *J. Phys.* D: *Appl. Phys.* **41**, 1–10.